Multi-Pass Performance of a Chip-Enhanced WSS for Nyquist-WDM Sub-band Switching

Bill Corcoran, *Member, IEEE*, Chen Zhu, *Member, IEEE*, Jochen Schröder, *Member, IEEE*, Leimeng Zhuang, Benjamin Foo, *Student Member, IEEE*, Maurizio Burla, Willem P. Beeker, Arne Leinse, Chris G.H. Roeloffzen, and Arthur J. Lowery, *Fellow, IEEE, Member, OSA*

***Abstract*— We investigate the performance of a chip-enhanced wavelength selective switch (EWSS) in multi-pass add/drop experiments. The demonstrated EWSS device uses a ring-assisted Mach-Zehnder interferometer chip as a wavelength interleaver, to pre-process the incoming super-channel before launch into a commercial wavelength selective switch. We show that a 4% guard-band, QPSK encoded Nyquist WDM super-channel can successfully pass through 7 EWSS nodes. We further investigate the number of reachable nodes with varied guard-bands, showing that a modest increase in guard-band can translate to a significant increase in the number of reachable EWSS nodes.**

***Index Terms*—Optical Communications, Wavelength Selective Switching, Optical Super-Channels, Photonic Integration, Ring Resonator, Optical Filters, Nyquist WDM, Reconfigurable Optical Add /Drop Multiplexing, Optically Routed Networks**

I. Introduction

OPTICAL super-channels allow for full spectral occupancy, maximizing spectral efficiency in fiber optic communication systems [1,2]. These densely-packed, wavelength division multiplexing (WDM) systems are typified by having little to no guard-band between channels. This then provides challenges for the use of super-channels in optically routed systems, as the filtering functions provided by common wavelength selective switches (WSSs) are limited in resolution by Gaussian optical transfer functions (OTFs) of close to 10 GHz in width [3,4]. The limited OTF causes a roll-off for WSS filters in the range of 10s of GHz [3,5], which leads to transition bands on a 50-GHz grid of >20%, effectively negating the spectral efficiency gains made by utilizing super-channels.

This problem has led to the demonstration of a number of methods to allow for wavelength selective switching and add/drop multiplexing of sub-bands (or sub-carriers) within optical super-channels. In the case of orthogonal frequency division multiplexing (OFDM) based super-channels, methods based on interference-based nulling of individual sub-carriers has been trialed successfully. These approaches are typically complex, involving a high resolution, full coherent transceiver [6] or optical clock recovery and fast sampling [7], due the difficulty of wavelength de-multiplexing sub-carriers with overlapping spectral components.

This constraint can be eased by either splitting an OFDM super-channel up into multiple sub-bands [8] or by taking advantage of the rectangular sub-band spectral shape that is provided in a Nyquist-WDM (NWDM) super-channel [2]. Add/drop multiplexing of bands within a multi-band OFDM signal has recently been shown using a stimulated Brillouin scattering filter [9]. While the generated filter has very sharp roll-off, the achievable filter bandwidth is limited to ~1 GHz. This bandwidth limit was circumvented in [10] by using an arrayed waveguide grating as a highly dispersive element in an modified 4-f spectral phase filter, and de-multiplexing of OFDM sub-bands was successfully demonstrated. However, the cyclic nature of the arrayed waveguide grating limited the operating bandwidth of this device to a single 250-GHz free-spectral range. Apart from arrayed waveguide gratings, other photonic chip based platforms have also been investigated to provide filters with sufficient resolution to separate out NWDM sub-bands, with Nyquist pulse shaping demonstrated [11]. This chip-based filter can be potentially operated over the entire C-band, as opposed to 250-GHz in [10]. However, as the filter design in [11] is fundamentally based on a finite-impulse response (FIR) structure, a large number of relatively long delays (i.e. 10s of bit-periods) are required. This provides difficulties with respect to fabrication tolerances, and also to the stability of tuning each waveguide element to the required state.

Here we use a chip-based wavelength interleaver, based on

Submitted xx October 2015. This work was supported by Laureate Fellow (LF130100041), DECRA (DE120101329) and Centres of Excellence (CE110001018) schemes of the Australian Research Council. We thank Finisar Australia for the 2×1×14 WSS.

B. Corcoran, C. Zhu, L. Zhuang, B. Foo and A.J. Lowery are with the Dept. of Electrical and Computer Systems Engineering, Monash Univeristy, VIC 3800, Australia (e-mail: {bill.corcoran; chen.zhu; leimeng.zhuang; benjamin.foo; arthur.lowey} @ monash.edu).

J. Schröder is with the School of Electrical and Computer Engineering, RMIT University, Melbourne, VIC 3000, Australia (email: jochen.schroeder@rmit.edu.au).

M. Burla was with the Institut National de la Recherche Scientifique (INRS-EMT), Montréal, Canada and is now at the Institute of Electromagnetic Fields, ETH Zurich, Zurich, Switzerland (e-mail: maurizio.burla@ief.ee.ethz.ch),

W.P. Beeker and A. Leinse are with LioniX BV, PO Box 456, Enschede, 7500 AL, the Netherlands (e-mail: willem.beeker@gmail.com; a.leinse@lionixbv.nl).

C.G.H Roeloffzen is with SATRAX BV, PO Box 456, Enschede, 7500 AL, the Netherlands (e-mail: c.g.h.roeloffzen@satrax.nl).

an infinite-impulse response (IIR) design [12], as a high resolution pre-filter before a commercial WSS module [13]. The ring-assisted Mach-Zehnder interferometer (RAMZI) interleaver chip provides rectangular shaped filters [12,14-17], separating out odd and even sub-bands, while the 2×1×14 WSS module is able to provide reconfigurable switching capability. Previously, we have shown that this chip enhanced WSS (EWSS) is capable of switching 12-GHz sub-bands out of a 4% guard-band NWDM super-channel, allowing for add /drop multiplexing within super-channels [18]. Here we extend our work presented at ECOC 2015 to explore the limitations of this device as a WSS in a fiber link, by measuring the performance of processed channels after multiple passes through the EWSS. We find that with QPSK encoded data, the EWSS filtering causes <1dB penalty in back-to-back transmission for a 4% guard-band signal, and allows for 7 hops in a link consisting of 100-km fiber spans with an EWSS at each node. We also sweep the guard-band percentage from 4 to 33%, finding that above 20%, signal distortions due to filtering are minimized.

In Section II we describe the EWSS structure and basic capabilities, Section III evaluates the performance of the EWSS in a model transmission system, Section IV discusses future improvements and the outlook for our approach.

This demonstration shows that sub-band access in optical super-channels can be made possible with devices retro-fitted to currently installed WSS units, and opens up the possibility of providing flexible, elastic fiber optic networks with very high spectral occupancy and efficiency.

II. Chip-Enhanced Wavelength Selective Switch

The basic principle of the EWSS device is to pre-filter the incoming optical signal using an interleaver with high spectral resolution, but with a channel separation able to be individually addressed by an off-the-shelf WSS. The odd and even bands coming out of the interleaver can be processed separately by the WSS, then the separately processed outputs are passively recombined to reform a super-channel.

The RAMZI interleaver [12, 14-17] chip used provides a

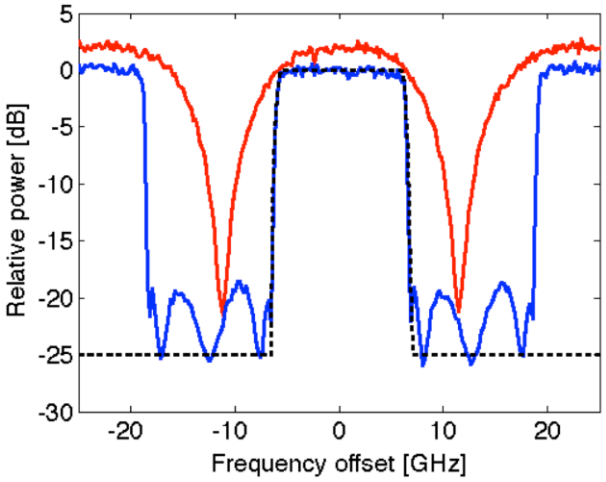

Fig. 1. Filter functions for the RAMZI chip (blue) and LCoS WSS (red). Measured with a 15-MHz resolution optical spectrum analyzer. For comparison, the black dotted line is for an 8% roll-off, 25-dB stop-band attenuation RRC filter.

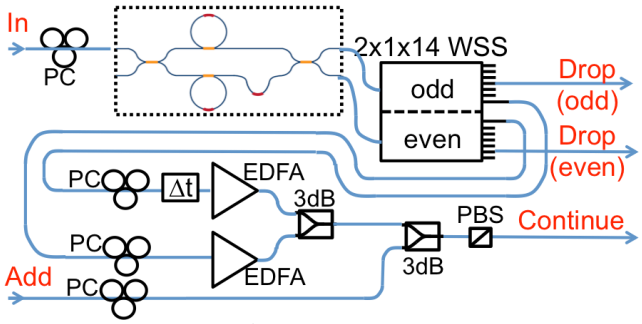

Fig. 2. Experimental set-up for the EWSS, showing input, drop, continue and add ports. PC: Polarization controller, EDFA: Erbium-doped fiber amplifier, PBS: Polarization beam splitter. '3dB' denotes coupler power splitting ratio, 'Δt' denotes a delay.

12.5/25-GHz banding, with pass-band 3-dB widths of 12.5 GHz, rolling off to -25 dB transmission over close to 1-GHz, giving an excess bandwidth of 8%. In comparison with the pass-band resolution figure given in [10,19], defined there as the 10%-90% (-0.5-dB to -10-dB) bandwidth, the RAMZI interleaver gives approximately 0.5-GHz resolution.

The interleaver's response can be modeled by using a z-transform-based formulation [12,14,15], and is similar to a root-raised cosine (RRC) filter with 8% roll-off and 25-dB stop-band attenuation, comparable to the digital filters used for the generation of NWDM sub-bands. The center frequency of the pass-bands can be thermally tuned on this chip, but the grid is fixed by the path lengths within the RAMZI.

The WSS used is a single module housing two separate WSS units – a 2×1×14 WSS – with both WSS units using a liquid crystal-on-silicon (LCoS), 4-f-type spectral-phase filter as a switching element [13]. Similar devices are commercially produced as WSSs for reconfigurable optical add/drop multiplexers (ROADMs). The resolution of the devices is limited by their OTFs to close to 10 GHz [3]; however, this is sufficient to define separate add or drop bands for the 12.5-GHz spaced outputs of the odd or even ports of the interleaver. A comparison of the interleaver chip and WSS transfer functions is shown in Fig. 1.

Fig. 2 shows the experimental set-up for the EWSS. As the RAMZI interleaver chip used in experiment has >10 dB polarization dependent insertion loss (i.e. optimized for single polarization operation), polarization control is required at various stages in the set-up. The interleaved outputs of the chip pass to the 2×1×14 WSS. The processed WSS outputs are either routed to a selection of drop ports, or to a designated continue port. The two separate odd and even continue ports are polarization controlled, and passively recombined in a 3-dB optical coupler. Polarization alignment of the odd and even channels at the continue output of the EWSS is ensured by passing the combined signal through a polarization beam splitter (PBS). This allows the EWSS to demonstrate drop and continue functions for NWDM sub-bands.

In addition to drop and continue, an add function is emulated by passive combination. Ideally, this would be achieved by using either an additional EWSS, or 2×*N*×14 WSS to allow for full ROADM configuration. Here, we simply add in an additional NWDM band to the EWSS

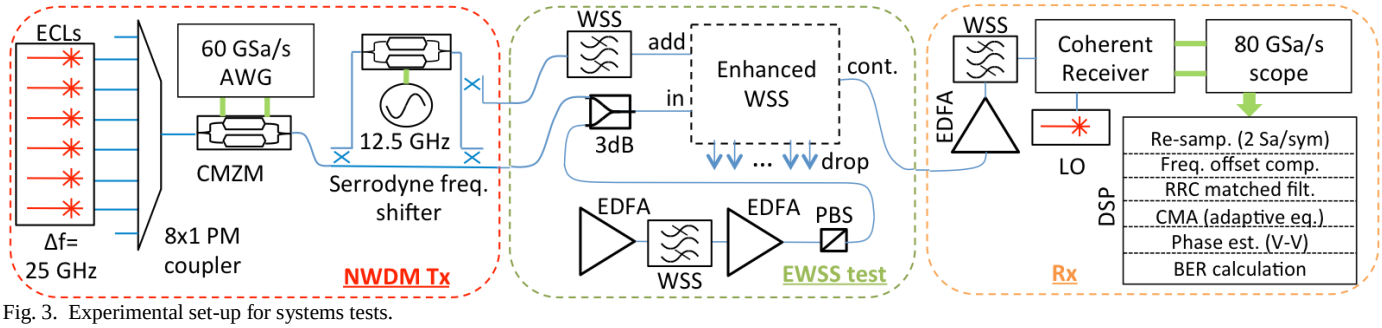

Fig. 3. Experimental set-up for systems tests.

processed super-channel with a 3-dB coupler.

In this set-up, the chip provides close to 12-dB fiber-to-fiber insertion loss (IL), the WSS around 5 dB, with other components providing 7-8-dB IL for a total IL of 25 dB. In Fig 2, the EWSS loss is split by amplification directly after the chip, effectively providing two separate loss stages of close to 12 dB.

Losses in this set-up can be reduced. The chip used here is fabricated from Lionix's TriPleX™ Si_3N_4-SiO_2 platform [20], which with careful end-facet design, waveguide geometry tuning and fiber coupling is predicted to reduce losses to close to 3 dB [15,20,21]. New hardware revisions of LCoS-based WSS to a 4×16 WSS provide similar insertion loss, with typical values of 4.5 dB [22]. However, by using this type of WSS, the need for passive combination with 3-dB couplers would be removed, lowering other component losses to < 1 dB, for a total estimated EWSS insertion loss of 8.5 dB. Practically, in our demonstration, we place erbium-doped fiber amplifiers (EDFAs) after the odd and even outputs of the chip to mitigate the effects of losses.

Note that in the set-up described in Fig. 2, the odd and even outputs are delayed relative to one another. This is to ensure de-correlation between the signal and interference from the other interleaved band when re-combining odd and even bands. Due to the fiber connecting the chip to the WSS, in our set-up there will be a random phase drift between odd and even bands, such that the 'interference' from the other band will alternately constructively or destructively interfere with the signal if the two paths are temporally synchronized. We add in a > 100-symbol de-correlating delay to in our set-up to produce a stable output, even though this does provide the maximum amount of interference between all sub-bands.

III. System Performance

In order to test the performance of the EWSS, we pass through a 150-GHz bandwidth, quadrature-phase-shift-keying (QPSK) encoded NWDM super-channel and measure signal quality at output. The experimental set-up is shown in Fig. 3.

The transmitter consists of a bank of external cavity lasers (ECLs), a single complex Mach-Zehnder modulator (CMZM) producing QPSK encoded NWDM bands and a serrodyne frequency shifting stage to produce a super-channel with delay de-correlated odd and even sub-bands.

The 6 independent ECLs are spaced 25-GHz apart, and are combined together using a polarization maintaining 1×8 coupler. These combined lines are then modulated using a 20-GHz bandwidth dual-nested Mach-Zehnder modulator, driven by waveforms generated from a 60 GSa/s, 20-GHz bandwidth arbitrary waveform generator (AWG). The AWG waveforms are pre-emphasized to flatten the combined frequency response of the components used in the system, and produce NWDM bands with 1% roll-off, at baud rates at or below 12 GHz. This produces correlated data on bands spaced by 25 GHz. The modulator output is amplified using a polarization maintaining EDFA directly after the modulator, then split by a 3-dB coupler, with one output serrodyne frequency shifted by 12.5-GHz via a second CMZM, amplified and delayed with respect to the other 3-dB coupler output. The two arms are then passively re-combined by another 3-dB coupler to produce a single polarization, 14-sub-band super-channel, with the guard-band defined by the ratio of the sub-band baud-rate to the 12.5 GHz sub-band spacing. With a 4% guard-band and assuming a 7% forward error correction (FEC) overhead, this produces a 270 Gb/s net (288 Gb/s gross) rate super-channel in a single polarization (at 1.8 b/s/pol.). Before frequency shifting, a portion of the original signal is tapped off and filtered with a 1×4 WSS to isolate a single NWDM sub-band for use as an 'add' sub-band.

Noise is loaded in a single polarization matched to that of the transmitter. Alignment is assured by passing the generated noise through a polarizing beam splitter, where the output is coupled to polarization maintaining fiber, and the signal and noise coupled using a polarization maintaining 3-dB coupler. A portion of the power of the subsequent noise loaded output is measured using an optical spectrum analyzer (OSA) set to 0.1-nm (12.5-GHz) resolution. In band OSNR is inferred from the measured spectrum using out-of-band measured noise powers.

The receiver consists of an EDFA pre-amplification stage, a 40-GHz bandwidth optical filter centered on the sub-band to be measured, and a coherent receiver. The coherent receiver uses an ECL as a local oscillator, which with the signal is coupled into an integrated package with an optical hybrid and balanced photodiodes. The photodiodes are AC coupled with a 25 GHz specified bandwidth. The balanced photodiode output is digitized with an 80-GSa/s, 33-GHz real-time oscilloscope. The digitized waveforms are processed offline.

The digital signal processing (DSP) used for signal recovery consists of receiver I/Q imbalance correction, residual-carrier based frequency offset estimation, overlap-add chromatic dispersion compensation, training aided synchronization, matched filtering with a 1% roll-off, 25-dB stop-band attenuation RRC filter, adaptive equalization based on the constant-modulus algorithm (CMA), Viterbi-Viterbi phase

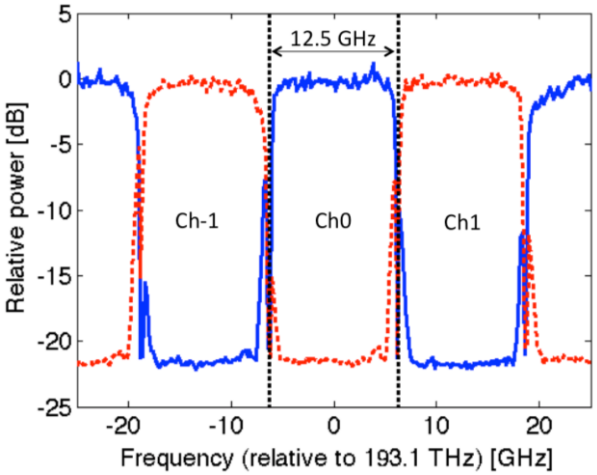

Fig. 4. Signal spectra at the odd (solid blue) and even (dashed red) outputs of the EWSS continue ports, with a 4% guard-band, NWDM super-channel input. A single 12.5-GHz sub-band slot is denoted by the black dotted lines, defining the in-band region for signal-to-interference ratio measurement.

estimation, maximum likelihood demodulation and, finally, error counting.

A. *Performance with noise loading*

We first test the basic function of the EWSS in a back-to-back test. Fig. 4 shows the generated super-channel with 4% guard-band (12-Gbd sub-bands spaced at 12.5 GHz), at the odd and even outputs of the WSS. Analyzing the odd and even outputs, we can estimate the interference power by summing (for example) the residual signal power in the odd bands of the even output. We define the signal-to-interference ratio as the total in-band signal power from the odd (even) port to the total in-band interference power coupled in from the even (odd) port. From Fig. 4 we estimate this ratio to be 21 dB.

Fig. 5 shows the performance of the two middle sub-bands of the super-channel against the loaded optical signal-to-noise ratio (OSNR), with and without passing through the EWSS. Here, we measure the quality factor (Q=10log$_{10}$($\sqrt{[}\mu^2/\sigma^2]$)) of the signal, as measured from the mean (μ) and variance (σ^2) of the constellation points, with the mean values taken from the modulated symbols. This measure compares well with Q extracted from the bit-error rate (BER) as Q=20log$_{10}$($\sqrt{2}$erfc^{-1}[2×BER]) when there are sufficient errors measured.

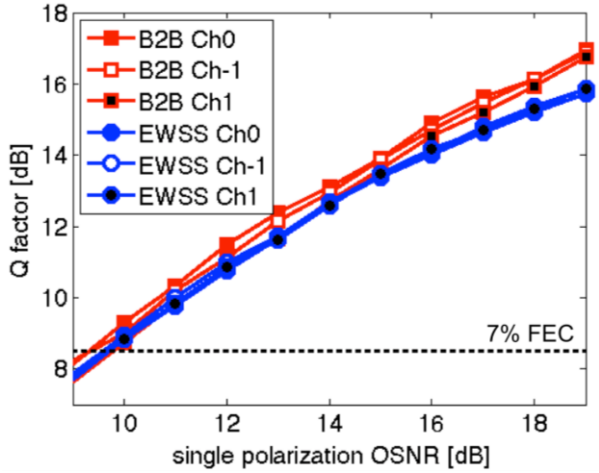

Fig. 5. Performance under noise loading for three center sub-bands, before (B2B) and after (post-EWSS) processing in EWSS (all sub-bands set to continue). Sub-band 0 (Ch0) is at 193.1 THz, Sub-bands 1 and -1 (Ch1, Ch-1) are the nearest neighbors, shifted by 12.5 GHz compared to Ch0.

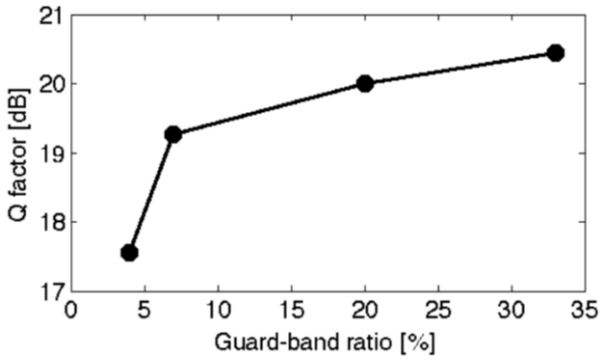

Fig. 6. Performance of center sub-band, with varied guard band ratios. Single EWSS pass, all sub-bands set to continue, no noise loading.

At high OSNRs, the post-EWSS trends approach a lower value of Q than for the same sub-bands before processing ('back-to-back', marked as B2B in Fig. 5). This difference is likely to be due to interference when the odd and even channels are recombined after the WSS. At lower OSNRs, the difference in performance between the B2B and post-EWSS traces reduces, such that near the 7% hard-decision FEC threshold (Q = 8.56) we find that the post-EWSS bands need on average only an extra 0.3-dB OSNR than bands before processing. This indicates that in a noise limited system the addition of a single EWSS has only a minor effect of system performance.

The experiments in [18] and those shown in Fig. 5 all used a 4% guard-band super-channel as the test signal. A common arrangement for current 100-Gb/s DWDM PM-QPSK systems uses 32-Gbd signals on a 50-GHz grid, providing an effective guard-band of 36%. As such, the effect of changing guard-bands for the NWDM 'super-channel' was investigated by setting the baud rate to 11.6, 10 and 8.25 Gbd, corresponding to guard-bands of 7%, 20% and 33%, respectively. In this case, the signal first propagates through a single, 100-km long span of standard single-mode fiber (SSMF), and is then amplified before processing in the EWSS. This is done without prior noise loading. The performance of the central sub-band at various guard-band ratios (baud rates) is shown in Fig. 6. We see that as the guard-band is increased (baud rate is

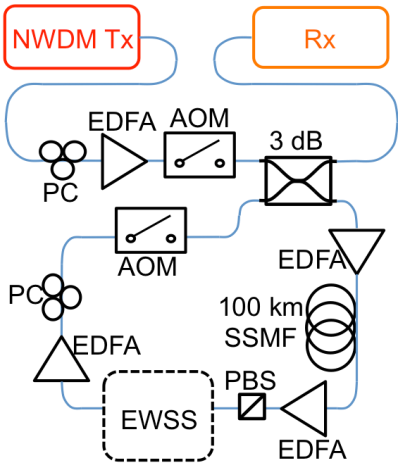

Fig. 7. Experimental set-up for multiple passes through the EWSS, using a fiber recirculating loop. The sub-systems 'NWDM Tx', 'Rx', and 'EWSS are as described in Figs. 2 & 3. AOM: Acousto-optic modulator, SSMF: standard single-mode fiber.

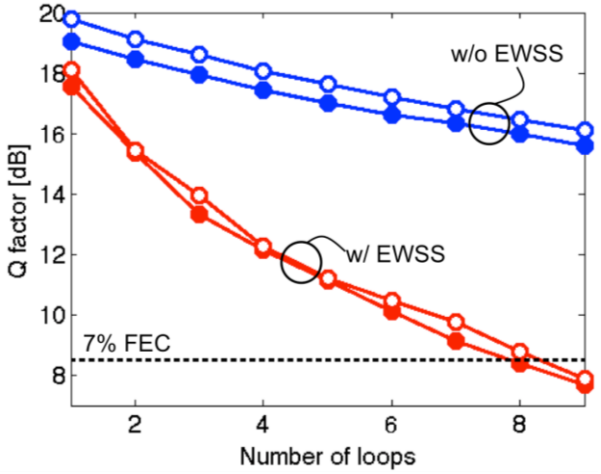

Fig. 8. Loop performance for center sub-bands (solid: Ch0, open: Ch-1) for 4% guard-band, with (w/) or without (w/o) the EWSS. The EWSS is set to continue all sub-bands. For the 'w/o EWSS' trace, the EWSS is replaced with a 200-GHz band-pass filter.

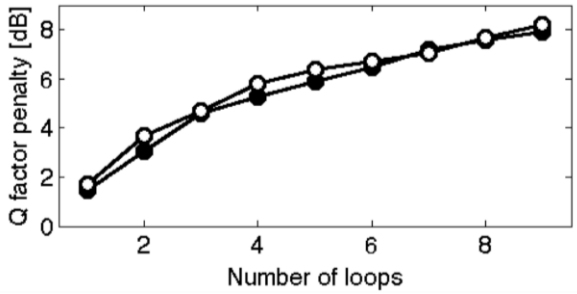

Fig. 9. Relative penalty after multiple EWSS passes compared to loop performance without the EWSS for the center two sub-bands (solid: Ch0, open: Ch-1), extracted from the data in Fig. 8.

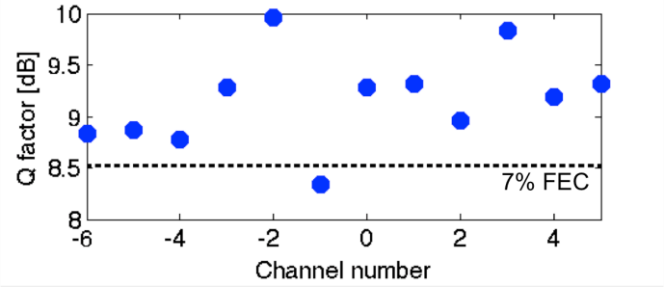

Fig. 10. Per-sub-band performance after 7 loops. EWSS is set to continue all sub-bands.

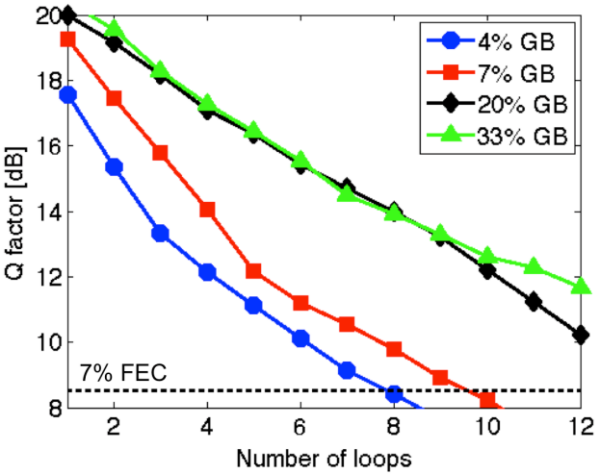

Fig. 11. Loop performance of center sub-band (Ch0) after EWSS (all-sub bands to continue). The guard-band ratio was varied by changing sub-band baud rate with a constant 12.5-GHs spacing.

decreased), performance improves. As there is no noise loading, and we have a high oversampling rate that both transmitter and receivers, we expect that this improvement indicates that the inter-sub-band interference is stronger near the edges of the interleaver bands (see Fig. 4), so that the higher guard-band ratio signals experience less interference. There may also be effects from the pass-band of the EWSS being slightly curved, such that the signal components closer to the edge are slightly more attenuated, lowering sub-band performance slightly.

B. Performance with multi-hop transmission

In an optical network, signals may pass through several ROADM/WSS stages between transmitter and receiver. We emulated this situation by placing the EWSS in a recirculating loop with a 100-km long span of SSMF and an EDFA for power regeneration. The experimental set-up for this is shown in Fig 7. Here, we emulate a network with an EWSS placed at each node between fiber spans. This allows the signal degradation to be dominated by impairments from filtering in the EWSS, providing an indication of the number of EWSS nodes able to be passed. From Figs. 4 and 6, we infer that the main cause of impairment is cross-talk through the RAMZI interleaver, although there may also be effects from pass-band shaping.

The performance for the two center sub-bands of the 4% guard-band super-channel, with either the EWSS or a 200-GHz band-pass filter in place, is plotted against the number of loops (spans and EWSS nodes passed) in Fig. 8. Without the EWSS in place, *Q* drops from around 19.5 dB to 16.5 dB, primarily due to accumulated noise. In this case, the launch power into the SSMF span was set to provide near optimal performance, set to 4 dBm. This launch power figure was kept the same for all of the following loop measurements.

With the EWSS in place, channel performance decreases at a greater rate, and remains above the FEC threshold for 7 loops. Fig. 9 shows the relative degradation between the two set-ups, showing that the EWSS degrades performance by about 1.6 dB after a single hop, increasing to an 8-dB degradation in *Q* after 9 hops. As expected, degradation from passing through the EWSS is greatest in the first few hops, and reduces with subsequent hops as the additional interference power from each subsequent pass is a lower proportion of the total interference power.

To gauge the uniformity of sub-band performance, the *Q*-factor of each of the sub-bands is measured after 7 loops, as shown in Fig. 10. Here *Q* is calculated from BER as > 100 errors are measured for all points. Most channels exceed the 7% hard FEC threshold, excepting sub-band -1. The measured *Q* shows a maximum variation of ±0.8 dB, with *Q* calculated from mean BER as 9.1 dB. This variation is comparable to our previously shown back-to-back, noise loaded results shown in [18], where a variation between sub-band performance of ±0.7 dB was measured close to the FEC limit.

As with the single-pass case shown in Fig. 6, the guard-band between sub-channels can be varied to illustrate how interference accumulation changes with increasing guard-band ratios. Fig. 11 shows the performance of the center sub-band against number of hops for varied guard-band ratios (different

sub-band baud rates). The performance above the 7% FEC threshold is limited to 7 hops for 4% guard-band, increasing to 9 hops for 7% guard-band. The higher 20% and 33% guard-band ratio signals remain well above the FEC threshold after 12 hops. The 33% guard-band result is close to the commonly used signal to channel spacing ratio of 32-Gbd signals on a 50-GHz grid (i.e. 36%), with the smaller band spacing shown here improving upon the typical spectral occupancy of current DWDM systems. This indicates that the EWSS we demonstrate here can be not only used for very low guard band super-channels, but also to generally enhance the spectral occupancy in optically routed systems compared to current systems.

IV. Discussion

There are several ways in which to improve upon the current EWSS system in terms of both function and performance. Pathways for the reduction of losses were discussed in Section II, which are necessary to make the EWSS useful as part of an optically routed network.

Apart from loss reduction, the current chip that we use requires a considerable power to tune the separate elements of the RAMZI circuit to form the required interleaver functionality, due to the original application of this circuit as a part of a reconfigurable device for microwave photonics [20,23]. Fabricating a device that targets the specific phase shifts and coupling factors that are needed for the interleaver configuration could significantly reduce power consumption. New, strain-based tuning methods also offer exceptional power efficiency [24].

The chip that we used can only support operation in a single polarization state, which is problematic considering that the input state of polarization is likely to be random and the signals to be processed likely to be polarization multiplexed. Polarization diversity, using two RAMZI filters is one obvious solution to this problem. Polarization diverse devices have been demonstrated on silicon-based integrated circuit platforms (e.g. [25,26]). Although careful matching of the two RAMZI responses would be necessary, the low component count in this filter design allows us to consider diversity as an option. We expect small phase and timing offsets of the two paths would be taken care of with common polarization tracking receiver-side DSP.

The placement of the chip within the EWSS is not necessarily optimal. Currently, as the out-of-band components of each interleaver are delay de-correlated from the other interleaver band, each pass through the EWSS adds in a significant amount of interference. This may be negated by placing the chip directly at the front end of the phase stable LCoS 4-f spectral phase filter within the WSS, not dissimilar to the placement of an arrayed-waveguide grating chip within an LCoS based device in [10]. We would imagine that the continue bands would then experience a much reduced amount of interference, allowing for a greater number of passes through ROADM/WSS nodes incorporating an EWSS.

The design of the RAMZI interleaver can also be extended to higher orders (i.e. adding more rings into the design) to give sharper roll-off characteristics [27]. However, this will come with an increase in fabrication and control complexity, and may prove difficult to configure correctly.

The current EWSS incorporates 12.5-GHz bands on a 25-GHz grid (i.e. a 12.5/25-GHz interleaver). While this is compatible with the WSS that we used, there is scope for change of the circuit parameters. A finer granularity, using a 10/20-GHz interleaver would also be possible, although as the odd-even band spacing is narrowed, achievable out-of-band rejection through the WSS switching will decrease. This trade-off of the interleaver granularity and WSS resolution requires further investigation. Moreover, coarser granularity is also possible, which would still allow for a reduction in achievable guard-band. For instance, the pass-band shape of a RAMZI with 8% excess bandwidth of a 50/100-GHz interleaver would still have a faster roll-off than a 10-GHz Gaussian OTF provided by an LCoS WSS. Wider pass-bands would require shorter path lengths in the RAMZI, and so should be less sensitive to fabrication imperfections (i.e. phase errors) that the chip we use here.

The RAMZI architecture used requires only standard photonic integrated circuit building blocks available through established photonic chip foundries [28, 29], providing the possibility for near-term mass-manufacture of the required interleaver pre-filter. Moreover, by using an off-the-shelf WSS as our switching engine, the addition of the interleaver chip as a retro-fit to current devices is enabled. This indicates that the proposed EWSS system may not require extensive further development before potential deployment.

In summary, while our demonstration does provide the ability to wavelength switch Nyquist-WDM sub-bands, there are several paths to improve the performance of our EWSS, toward creating a system of practical use in optically routed systems.

V. Conclusion

We have characterized the performance of a chip-enhanced wavelength selective switch capable of sub-band wavelength switching in a tightly packed, 4% guard-band, NWDM super-channel, in a model optically routed link. This super-channel was able to pass through seven EWSS nodes, and increasing the allowed guard-band ratio can extend the range of transmission to several more nodes. Our demonstration shows that it is possible to create devices that enable optically routed systems with the overall spectral occupancy of super-channels.

References

[1] W. Sheih & C. Athaudage, “Coherent optical orthogonal frequency division multiplexing,” *Electron. Lett.*, vol. 42, pp. 587, 2006.

[2] G. Bosco *et al.*, ““Performance limits of Nyquist-WDM and CO-OFDM in high-speed PM-QPSK systems”, *Photon. Tech. Lett.*, vol. 22, pp. 1129, 2010.

[3] C. Pulikkaseril *et al.*, “Spectral modeling of channel band shapes in wavelength selective switches”, vol. 19, pp. 8458, 2011

[4] D.M. Marom *et al.*, “Wavelength-selective 1xK switches using free-space optics and MEMS micromirrors: Theory, design, and implementation,” *J. Lightwave Technol.*, vol. 23, p. 1620, 2005.

[5] F. Heismann, “System requirements for WSS filter shape in cascaded ROADM networks,” in *Proc. OFC*, 2010, OThR1

[6] T. Richter *et al.*, “Coherent in-line substitution of OFDM subcarriers using fiber-frequency conversion and free-running lasers,” in *Proc. OFC*, 2014, Th5B.6.

[7] S. Fabbri *et al.*, "Experimental implementation of an all-optical interferometric drop, add, and extract multiplexer for superchannels," *J. Lightwave Technol.*, vol. 33, pp. 1351, 2015.
[8] W. Sheih, Q. Yang, Y. Ma, "107 Gb/s coherent optical OFDM transmission over 1000-km SSMF fiber using orthogonal band multiplexing", *Opt. Express*, vol. 16, pp. 6378, 2008.
[9] W. Wei *et al.*, "Ultra-selective flexible add-drop multiplexer using rectangular stimulated Brillouin scattering filters", in *Proc. OFC*, 2015, Tu3D.1.
[10] R. Rudnick *et al.*, "Sub-banded / single-sub-carrier drop-demux and flexible spectral shaping with a fine resolution photonic processor" in *Proc. ECOC*, 2014, PD.4.1.
[11] T. Goh *et al.*, "Optical Nyquist-filtering multi/ demultiplexer with PLC for 1-Tb/s class super-channel transceiver" in *Proc. OFC*, 2015 Tu3A.5.
[12] C.K. Madsen, "General IIR optical filter design for WDM applications using all-pass filters" *J. Lightwave Technol.*, vol. 18, pp. 860, 2000
[13] G. Baxter *et al.*, "Highly programmable wavelength selective switch based on liquid crystal on silicon switching elements" in *Proc. OFC*, 2006, OTuF2.
[14] L. Zhuang *et al.*, "Full-C-band, sub-GHz-resolution Nyquist-filtering (de)interleaver in photonic integrated circuit", http://arxiv.org/abs/1509.00564
[15] L. Zhuang *et al.*, "Novel wideband microwave polarization network using a fully-reconfigurable photonic waveguide interleaver with a two-ring resonator-assisted asymmetric Mach-Zehnder structure", *Opt. Express*, vol. 21, pp. 3114, 2013.
[16] Z. Wang *et al.*, "A high-performance ultracompact optical interleaver based on double-ring assisted Mach–Zehnder interferometer", Photon. Tech. Lett., vol. 19, pp 1072, 2007
[17] J. Song *et al.*, "Passive ring-assisted Mach-Zehnder interleaver on silicon-on-insulator", *Opt. Express*, vol. 16, pp. 8359, 2008
[18] B. Corcoran *et al.*, "A wavelength selective switch for optical add/drop multiplexing of sub-bands within Nyquist WDM super-channels" in *Proc. ECOC*, 2015, Tu3.5.2
[19] R. Rudnick *et al.*, "One GHz resolution arrayed waveguide grating Filter with LCoS phase compensation", in *Proc. OFC*, 2014, Tu3F.7
[20] C.G.H. Roeloffzen *at al.*, "Silicon nitride microwave photonic circuits", *Opt. Express*, vol. 21, pp. 22937, 2013
[21] Y. Fan *et al.*, "A hybrid semiconductor-glass waveguide laser," in *Proc. SPIE 9135, Laser Sources and Applications II*, 2014, 91351B
[22] Finisar Corp., "Waveshaper 16000S product brief", https://www.finisar.com/sites/default/files/downloads/waveshaper_16000s_product_brief_11_14_0.pdf, accessed 21 Oct. 2015
[23] M. Burla, D. A. I. Marpaung, L. Zhuang, M. R. Khan, A. Leinse, W. Beeker, M. Hoekman, R. G. Heideman, and C. G. H. Roeloffzen, "Multiwavelength-Integrated Optical Beamformer Based on Wavelength Division Multiplexing for 2-D Phased Array Antennas," J. Lightwave Technol., vol. 32, pp. 3509 (2014)
[24] N. Hosseini *et al.*, "Stress-optic modulator in TriPleX platform using a ezoelectric lead zirconate titanate (PZT) thin film," *Opt. Express*, vol. 23, pp. 14018 (2015)
[25] W. Sacher *et al.*, "Polarization rotator-splitters and controllers in a Si3N4-on-SOI integrated photonics platform", Opt. Express, vol. 22, pp. 11167 (2014)
[26] S.T. Chu, B.E. Little, V. Van, J.V. Hryniewicz, P.P. Absil, F.G. Johnson, D. Gill, O. King, F. Seiferth, M. Trakalo, J. Shanton, "Compact full C-band tunable filters for 50 GHz channel spacing based on high order micro-ring resonators," in Proc. OFC 2004 , xx.xx (2004)
[27] L. Zhuang *et al.*, "Ring-based interleaver for Nyquist filtering and WDM multiplexing", in *Proc. OFC*, 2015, Tu3A.6
[28] A. Khanna *et al.*,"ePIXfab: the silicon photonics platform," in *Proc. SPIE 8767, Integrated photonics: Materials, Devies and Applications II*, 2013, 87670H
[29] R.G. Heideman, "TriPleX™: The low loss passive photonics platform - Industrial applications through Multi Project Wafer runs", in *Proc. IPC*, 2014, TuC3.3